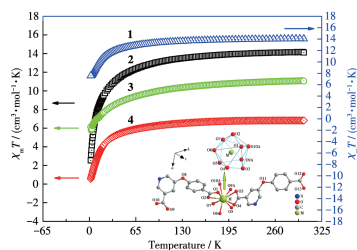


Synthesis, fluorescence, and magnetic characterization of nicotinic acid ligand-based dysprosium, holmium, erbium, and thulium complexes (English)

YU Lin-Tao, LI Qi-Yang, SHEN Zhi,
LÜ Wen-Jun, ZHAO Qiang

DOI:10.11862/CJIC.2023.187

Chinese J. Inorg. Chem., **2023**,**39**(00):-



It is found that 5-(4-carboxyphenoxy)nicotinic acid ligand forms isomorphous complexes with M^{3+} , where $M=Dy$ (**1**), Ho (**2**), Er (**3**), and Tm (**4**), and magnetic results indicate that the magnetism of all four complexes exhibits weak antiferromagnetic behavior.

基于多羧酸烟酸配体的镝、钬、铒和铥配合物的 合成及荧光、磁学性质的表征

于林涛 李奇洋 沈 芝 吕文君 赵 强*
(南阳师范学院化学与制药工程学院, 南阳 473061)

摘要: 以 5-(4-羧基苯氧基)烟酸配体(H_2cpna)和稀土金属离子 Dy^{3+} 、 Ho^{3+} 、 Er^{3+} 和 Tm^{3+} 为原料, 采用水热法合成了 4 种稀土金属配合物 $[M(Hcpna)(cpna)(H_2O)_3]_n$, 其中 $M=Dy$ (**1**)、 Ho (**2**)、 Er (**3**)、 Tm (**4**)。单晶 X 射线衍射分析表明配合物 **1**、**2**、**3** 和 **4** 为同构配合物, 均为一维链状结构。通过红外、元素分析以及粉末 X 射线衍射对所得配合物进行了表征, 同时对配合物的荧光和磁学性质开展了研究。荧光测试结果表明, 配合物 **1**~**4** 的荧光强度均低于配体 H_2cpna 的荧光强度。在 2~300 K 温度范围内 1 kOe 直流电场下测试了配合物 **1**~**4** 的磁性, 结果表明配合物 **1**、**2**、**3** 和 **4** 的 $\chi_m T$ 值分别为 14.04、14.15、11.08 和 6.83 $cm^3 \cdot mol^{-1} \cdot K$, 与文献理论值相符合。

关键词: 镝; 钬; 铒; 铥; 荧光; 磁性

中图分类号: O614.342; O614.343; O614.344; O614.345

文献标识码: A

文章编号: 1001-4861(2023)00-0000-07

DOI: 10.11862/CJIC.2023.187

Synthesis, fluorescence, and magnetic characterization of nicotinic acid ligand-based dysprosium, holmium, erbium, and thulium complexes

YU Lin-Tao LI Qi-Yang SHEN Zhi LÜ Wen-Jun ZHAO Qiang*

(College of Chemistry and Pharmaceutical Engineering, Nanyang Normal University, Nanyang, Henan 473061, China)

Abstract: Four isomorphous rare earth complexes $[M(Hcpna)(cpna)(H_2O)_3]_n$, where $M=Dy$ (**1**), Ho (**2**), Er (**3**), Tm (**4**), have been synthesized by a solvothermal method based on 5-(4-carboxyphenoxy)nicotinic acid ligand (H_2cpna) and rare earth metal ions Dy^{3+} , Ho^{3+} , Er^{3+} , and Tm^{3+} . Single crystal X-ray diffraction analyses reveal that complexes **1**, **2**, **3**, and **4** are isostructural, and the structures are all 1D chain structures. The complexes were characterized by IR, elemental analysis, and powder X-ray diffraction, while the fluorescence and magnetic properties of the complexes were studied. The fluorescence test results show that the fluorescence intensity of complexes **1**~**4** were all lower than that of the H_2cpna ligand. The magnetism of complexes **1**~**4** were studied in the 2-300 K range at 1 kOe dc field. The $\chi_m T$ values of complexes **1**, **2**, **3**, and **4** were 14.04, 14.15, 11.08, and 6.83 $cm^3 \cdot mol^{-1} \cdot K$ respectively at room temperature. CCDC: 2151711, **1**; 2112781, **2**; 2112782, **3**; 2112783, **4**.

Keywords: dysprosium(III); holmium(III); erbium(III); thulium(III); fluorescence; magnetism

Rare earth metals are called “Industrial Monosodium Glutamate” and “Treasure House” of new materials in today’s society. They can form many different new materials with different properties, and many mate-

rials are widely used in all walks of life^[1-5]. As a special kind of inorganic ions, rare earth ions have excellent optical, electrical, and magnetic properties. Wilkinson and Brightan successfully synthesized the first rare

收稿日期: 2023-05-31。收修改稿日期: 2023-09-28。

河南省青年骨干教师资助项目(No.2020GGJS180)南阳师范学院培育项目(No.2023PY001)资助。

*通信联系人。E-mail: zhaoqiang0522@126.com

earth metal-organic complex (tricycline rare earth compound) in 1954, marking the birth of rare earth metal organic chemistry. After that, many excellent studies on rare earth complexes have been reported, so the research on rare earth coordination compounds is particularly important^[6-9]. Based on the 4*f* electronic structure of rare earth ions, rare earth complexes have important potential applications in optical, magnetic, and other fields. Among these properties, the magnetic properties of rare earth complexes have been extensively studied^[10-11]. The high magnetic moment and strong magnetic anisotropy of rare earth ions provide the basis for them as the magnetic functional unit of molecular nanomagnets. However, due to the changeable coordination configuration of rare earth ions, the reasonable design and synthesis of rare earth complexes are still very challenging. In this paper, we report our discovery of four new rare earth complexes based on Dy³⁺, Ho³⁺, Er³⁺, and Tm³⁺ and 5-(4-carboxyphenoxy) nicotinic acid ligand (H₂cpna)^[12-13]. Furthermore, the fluorescence and magnetic properties of the complexes were investigated at room temperature.

1 Experimental

1.1 Material and measurements

All chemicals of reagent grade were commercially available and used without purification. The H₂cpna ligand was purchased from Jinan Camolai Trading Company (Jinan, China); Dy(NO₃)₃·6H₂O, Ho(NO₃)₃·6H₂O, Er(NO₃)₃·6H₂O, and Tm(NO₃)₃·6H₂O were purchased from Shanghai Aladdin Biological Technology Co., Ltd (Shanghai, China). The experimental water was distilled water.

Elemental analyses (C, H, and N) were performed using a Perkin-Elmer 2400 element analyzer. IR spectra were recorded in a range of 400-4000 cm⁻¹ using a VECTOR-22 spectrometer using KBr discs. Powder X-ray diffraction (PXRD) patterns were recorded on a Bruker (D8 Advance) diffractometer for a Cu - target tube and a graphite monochromator (voltage: 40 kV, current: 40 mA, incident ray wavelength: 0.154 06 nm, scanning range: 5°-90°). The simulated PXRD patterns were obtained by the single-crystal data and diffraction-

crystal module of the Mercury program. A thermal analyzer (TG-DSC, STA449F3, Germany) was applied to investigate the thermal stability of the sample under a nitrogen atmosphere at a heating rate of 10 °C·min⁻¹. Fluorescence tests were carried out on a Varian Cary Eclipse fluorescence spectrometer. Magnetic data were collected by a Quantum Design SQUID-VSM magnetometer.

1.2 Synthesis of complexes [M(Hcpna)(cpna)(H₂O)₃]_n (M=Dy, Ho, Er, Tm)

A mixture of H₂cpna (0.25 mmol), M(NO₃)₃·6H₂O (0.5 mmol), NaOH (0.45 mmol), and distilled H₂O (10 mL) was stirred magnetically for 5 min at room temperature, then was sealed in a 25 mL Teflon-lined autoclave and heated to 120 °C at a rate of 10.8 °C·h⁻¹. After maintaining for 72 h, the reaction vessel was cooled to 20 °C at a rate of 5 °C·h⁻¹. Light yellow crystals were collected.

[Dy(Hcpna)(cpna)(H₂O)₃]_n (**1**): 45% yield based on H₂cpna. Elemental Anal. Calcd. for DyC₂₆H₂₁N₂O₁₃(%): C, 42.66; H, 2.89; N, 3.83. Found(%): C, 42.98; H, 2.61; N, 4.59. FTIR (KBr pellets, cm⁻¹): 1 684, 1 599, 1 551, 1 504, 1 463, 1 408, 1 315, 1 298, 1 259, 1 208, 1 163, 1 024, 963, 909, 878, 853, 794, 763, 707.

[Ho(Hcpna)(cpna)(H₂O)₃]_n (**2**): 76% yield based on H₂cpna. Elemental Anal. Calcd. for HoC₂₆H₂₁N₂O₁₃(%): C, 42.52; H, 2.88; N, 3.81. Found(%): C, 42.38; H, 2.91; N, 4.19. FTIR (KBr pellets, cm⁻¹): 1 685, 1 602, 1 545, 1 505, 1 460, 1 408, 1 316, 1 300, 1 259, 1 211, 1 179, 1 165, 1 025, 965, 905, 874, 854, 802, 769, 708.

[Er(Hcpna)(cpna)(H₂O)₃]_n (**3**): 63% yield based on H₂cpna. Elemental Anal. Calcd. for ErC₂₆H₂₁N₂O₁₃(%): C, 42.38; H, 2.87; N, 3.80. Found(%): C, 42.16; H, 3.06; N, 4.20. FTIR (KBr pellets, cm⁻¹): 1 682, 1 602, 1 546, 1 506, 1 459, 1 406, 1 316, 1 299, 1 258, 1 213, 1 179, 1 165, 1 025, 965, 905, 872, 857, 799, 766, 706.

[Tm(Hcpna)(cpna)(H₂O)₃]_n (**4**): 57% yield based on H₂cpna. Elemental Anal. Calcd. for TmC₂₆H₂₁N₂O₁₃(%): C, 42.29; H, 2.87; N, 3.79. Found(%): C, 42.58; H, 2.49; N, 3.63. FTIR (KBr pellets, cm⁻¹): 1 687, 1 601, 1 547, 1 507, 1 460, 1 407, 1 316, 1 301, 1 259, 1 215, 1 179, 1 165, 1 027, 965, 904, 875, 854, 801, 769, 706.

1.3 X-ray data collection and structure determinations

Single-crystal X-ray diffraction data for complexes **1-4** were collected on a Bruker SMART APEX- II CCD diffractometer equipped with a graphite-monochromated Mo $K\alpha$ radiation ($\lambda = 0.071\ 073$ nm) at 293(2) K using an ω - φ scan mode. Absorption corrections were applied by using the SADABS program^[14]. The structure was solved by direct methods and refined by full-

matrix least-squares techniques on F^2 with the SHELX-2018 package^[15]. The H atoms of the ligands were generated theoretically on the specific atoms and refined isotropically with fixed thermal factors. Detailed crystallographic data of complexes **1-4** are summarized in Table 1.

CCDC: 2151711, **1**; 2112781, **2**; 2112782, **3**; 2112783, **4**.

Table 1 Crystallographic data for complexes 1-4

Parameter	1	2	3	4
Chemical formula	DyC ₂₆ H ₂₁ N ₂ O ₁₃	HoC ₂₆ H ₂₁ N ₂ O ₁₃	ErC ₂₆ H ₂₁ N ₂ O ₁₃	TmC ₂₆ H ₂₁ N ₂ O ₁₃
Formula weight	731.95	734.38	736.71	738.38
Space group	$P\bar{1}$	$P\bar{1}$	$P\bar{1}$	$P\bar{1}$
a / nm	0.593 37(17)	0.591 11(12)	0.587 71(12)	0.587 62(8)
b / nm	1.252 0(4)	1.247 8(3)	1.244 2(3)	1.245 17(17)
c / nm	1.801 9(5)	1.795 0(4)	1.788 7(4)	1.789 5(3)
α / (°)	93.274(5)	93.280(3)	93. 313(4)	93.355(2)
β / (°)	98.093(5)	98.051(3)	98.104(4)	98.202(2)
γ / (°)	92.964(5)	92.851(3)	92.894(4)	92.990(2)
Volume / nm ³	1.320 7(7)	1.306 5(5)	1.290 5(5)	1.291 3(3)
Z	2	2	2	2
D_c / (g·cm ⁻³)	1.841	1.851	1.880	1.883
Indices ranges	$-7 \leq h \leq 6,$ $-14 \leq k \leq 14,$ $-16 \leq l \leq 21$	$-6 \leq h \leq 7,$ $-11 \leq k \leq 14,$ $-21 \leq l \leq 20$	$-6 \leq h \leq 6,$ $-14 \leq k \leq 14,$ $-21 \leq l \leq 19$	$-6 \leq h \leq 6,$ $-14 \leq k \leq 12,$ $-21 \leq l \leq 20$
$F(000)$	722	712	714	716
Reflection collected	6 768	6 723	6 599	6 837
Unique reflection	4 610	4 562	4 503	4 504
R_{int}	0.026 7	0.024 9	0.029 5	0.042 7
GOF on F^2	1.053	1.027	1.048	1.033
R, wR [$I > 2\sigma(I)$]	$R_1=0.034\ 6,$ $wR_2=0.073\ 1$	$R_1=0.031\ 3,$ $wR_2=0.079\ 5$	$R_1=0.035\ 5,$ $wR_2=0.076\ 6$	$R_1=0.046\ 1,$ $wR_2=0.116\ 1$
R, wR (all data)	$R_1=0.041\ 4,$ $wR_2=0.079\ 2$	$R_1=0.037\ 0,$ $wR_2=0.093\ 2$	$R_1=0.043\ 7,$ $wR_2=0.081\ 0$	$R_1=0.050\ 7,$ $wR_2=0.121\ 5$

2 Results and discussion

2.1 Crystal-structural description

The structures of complexes **1, 2, 3,** and **4** are the same, so structural analysis of the four complexes is performed by representing the central atoms of M. Single-crystal X-ray diffraction analysis reveals that the complex crystallizes in the triclinic crystal system with the $P\bar{1}$ space group. The asymmetric unit comprises

one M³⁺ ion, one fully deprotonated ligand cpna²⁻, one partially deprotonated ligand Hcpna⁻, and three coordinated water molecules. Thus, a nine-coordinated structure is formed. As shown in Fig. 1a, M³⁺ is arranged in a distorted single-cap square inverse prism, O3, O4, O5, and O9A form the bottom of the tetragonal body, O3, O6, O7, and O10A form the top of the tetragonal body and O2 is the top of the single cap. The completely deprotonated cpna²⁻ ligand adopts $\mu_2: \eta^1, \eta^1, \eta^1, \eta^1$

coordination mode, and the partially deprotonated ligand Hcpna⁻ ligand adopts $\mu_1: \eta^1, \eta^1$ coordination mode (Scheme 1). M³⁺ ion is coordinated by two O atoms (O3 and O4) from cpna⁻, four O atoms (O1, O2, O9A, and O10A) from cpna²⁻ and three O atoms (O5, O6, and O7) from water molecules. Each M³⁺ ion linked two adjacent M³⁺ ions through fully deprotonated cpna²⁻ and formed infinite zigzag chains along the *b*-axis. (Fig.1b)

In the complexes, the O—M—O angles are in the ranges of 51.06(11)° - 160.16(14)° (**1**), 51.45(12)° - 159.80(14)° (**2**), 51.63(12)° - 159.76(14)° (**3**), and 51.58(15)° - 159.18(19)° (**4**). The M—O bond lengths change from 0.233 1(4) to 0.289 7(5) nm for **1**, from 0.230 8(4) to 0.287 9(6) nm for **2**, from 0.229 4(4) to 0.278 5(6) nm for **3**, and from 0.230 1(4) to 0.285 8(7) nm for **4**. The organic ligand exhibits two kinds of coor-

dination modes: one carboxyl group on the benzene ring of the Hcpna⁻ ligand is not coordinated and another COO⁻ group on the pyridine ring adopts a bidentate mode. The Hcpna⁻ ligand shows a dihedral angle (between pyridyl and benzene rings) of 53.20° (**1**), 52.69° (**2**), 52.92° (**3**), and 52.50° (**4**), and the C—O_{ether}—C angle between two aromatic rings is 120.50° (**1**), 120.40° (**2**), 120.22° (**3**), and 121.34° (**4**). For the cpna²⁻ ligand, two COO⁻ groups adopt bidentate mode. The cpna²⁻ ligand shows a dihedral angle (between pyridyl and benzene rings) of 66.89° (**1**), 66.84° (**2**), 67.26° (**3**), and 67.63° (**4**), and the C—O_{ether}—C angle between two aromatic rings is 119.64° (**1**), 120.14° (**2**), 119.58° (**3**), and 120.03° (**4**). The distance between adjacent M³⁺ atoms is 1.252 nm (**1**), 1.248 nm (**2**), 1.244 nm (**3**), and 1.245 nm (**4**).

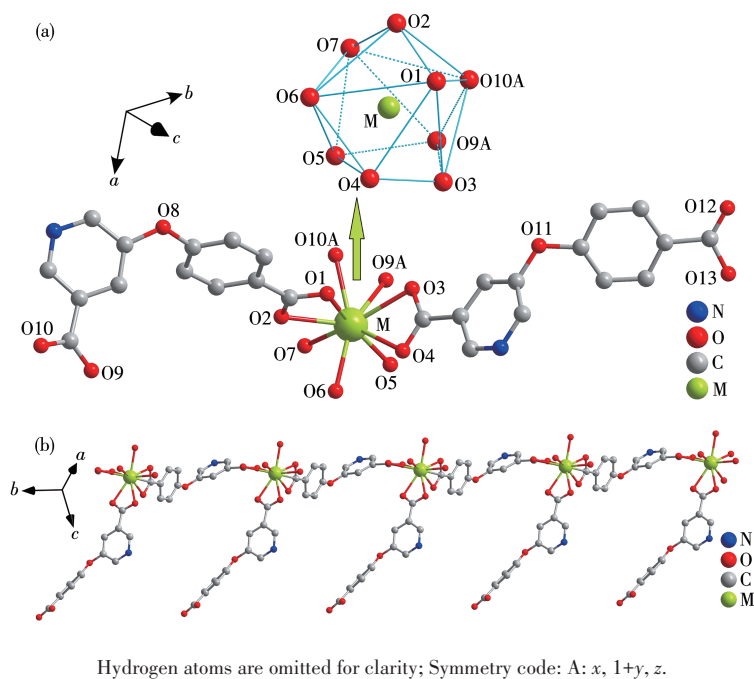
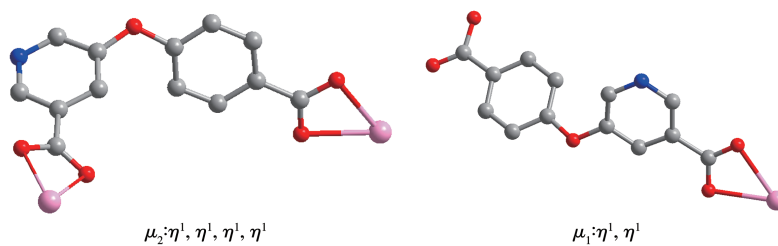


Fig.1 (a) Coordination environment of M³⁺ (M=Dy, Ho, Er, Tm) in complexes **1-4**; (b) 1D chain structure of complexes **1-4**



Scheme 1 Coordination modes of cpna²⁻ (left) and Hcpna⁻ (right) anions

2.2 PXRD analyses

PXRD analyses of complexes **1-4** were performed before the fluorescence and magnetic properties test. As shown in Fig.2, the experimental data are in good

agreement with the simulated pattern of single-crystal X-ray diffraction data, which proves that the phase purity of the test product is sufficient for the next step of the experiment.

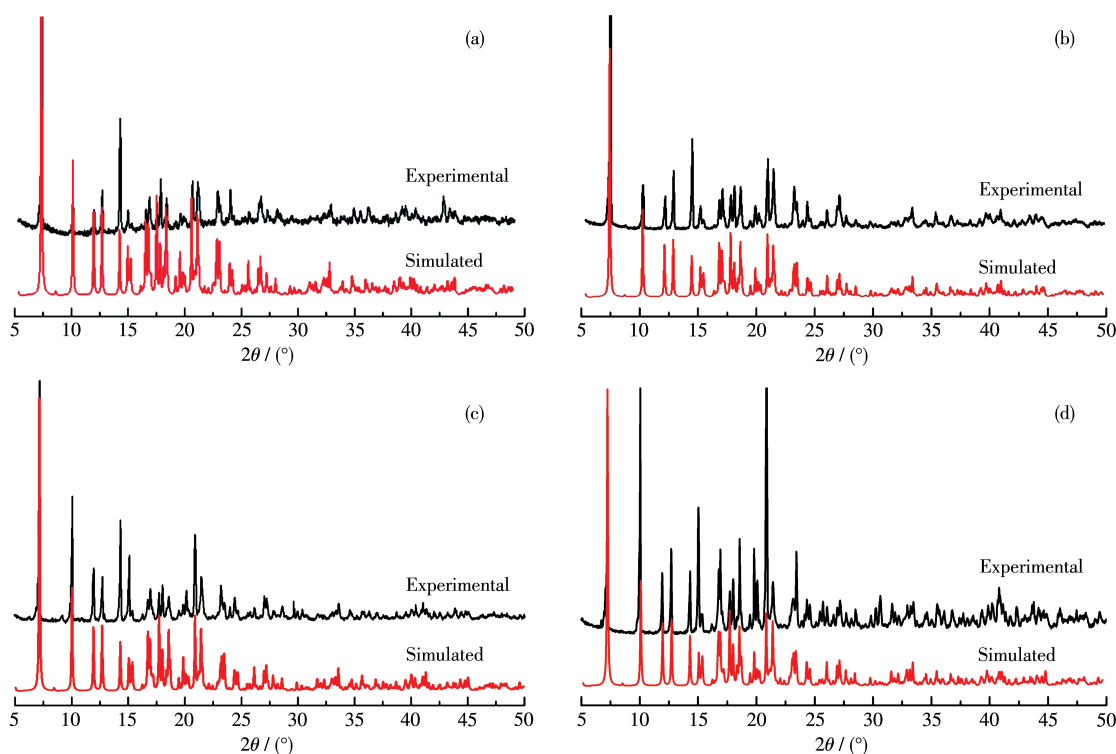


Fig.2 Experimental and simulated PXRD patterns of complexes **1** (a), **2** (b), **3** (c), and **4** (d)

2.3 TG analyses

To determine the thermal stability of the complexes, TGA experiments were carried out. As shown in Fig.3, the results of the TGA indicate that complexes **1-4** have almost the same thermodynamic stability. The complexes had two steps of decomposition in a range of 22-900 °C. The first major weight loss occurred at tem-

peratures between 22 and 200 °C corresponding to the removal of the water molecules. There was nearly no weight loss at the temperatures between 200 and 320 °C. The second weight loss occurred at temperatures between 320 and 900 °C, corresponding to the decomposition of the complex skeleton. TGA indicates complexes **1-4** have good thermal stability.

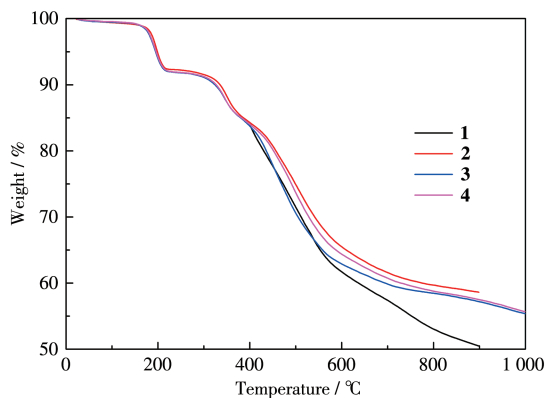


Fig.3 TGA curves of complexes **1-4**

2.4 Fluorescence spectrum

The solid-state fluorescence spectra of H₂cpna and complexes **1-4** were recorded at room temperature on a Varian Cary Eclipse fluorescence spectrometer under an excitation of 280 nm. As shown in Fig.4, the H₂cpna ligand had a wide emission band between 350 and 415 nm, and the maximum emission peak was about 390 nm. The emission peak of the ligand is attributed to the charge transfer within the ligand, that is, the electron transition of $n-\pi^*$ or $\pi-\pi^*$. The fluorescence test results show that complexes **1-4** had similar

fluorescence emission bands with the H₂cpna ligand. Therefore, it is considered that the fluorescence emission peak of the complexes comes from the ligand. The difference was that the fluorescence emission intensity of **1-4** were weaker than that of the ligand. After the formation of the complex, the lone pair electrons of the coordination atoms on the ligand form a coordination bond with the metal ions, which changes the electron distribution on the ligand. Coupled with the heavy atom effect of metal ions, the fluorescence intensity of the complex is reduced.

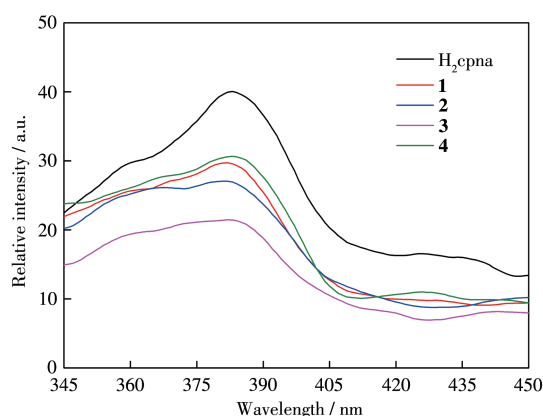


Fig.4 Fluorescence spectra of H₂cpna and complexes **1-4**

2.5 Magnetic properties

The magnetism of complexes **1-4** were studied on a Quantum Design SQUID-VSM magnetometer by solid-state magnetic susceptibility measurements in the 2-300 K range at 1 kOe dc field. Plots of the $\chi_m T$ versus T and magnetic analysis of complexes **1-4** are shown in Fig.5.

For complex **1**, $\chi_m T$ was almost a constant from 14.04 cm³·mol⁻¹·K at 300 K, corresponding to the

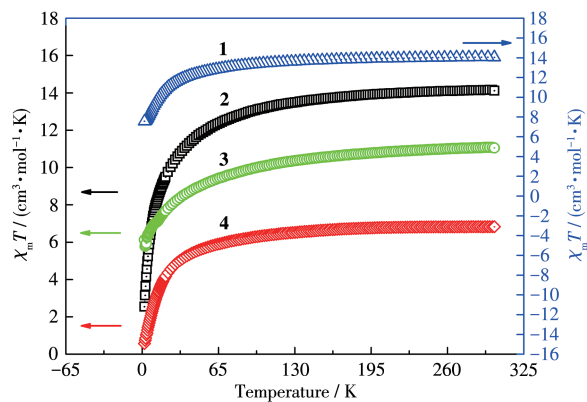


Fig.5 Plots of $\chi_m T$ vs T for complexes **1-4**

expected values (14.18 cm³·mol⁻¹·K) for one uncoupled Dy(III) ion^[16-17]. As the temperature decreased, $\chi_m T$ gradually decreased; reaching 7.56 cm³·mol⁻¹·K at 2 K. For complex **2**, $\chi_m T$ was almost a constant from 14.15 cm³·mol⁻¹·K at 300 K, which corresponds to the expected values (14.45 cm³·mol⁻¹·K) for one uncoupled Ho(III) ion^[18-19]. When the temperature decreased, $\chi_m T$ gradually decreased and reached 2.54 cm³·mol⁻¹·K at 2 K. For complex **3**, $\chi_m T$ value was 11.08 cm³·mol⁻¹·K at room temperature, which is consistent with the value (11.86 cm³·mol⁻¹·K) of one independent Er(III) ion^[20-21]. $\chi_m T$ gradually decreased as the temperature decreased, and finally reached 5.78 cm³·mol⁻¹·K at 2 K. For complex **4**, $\chi_m T$ was almost a constant from 6.83 cm³·mol⁻¹·K at 300 K, which is consistent with the value (7.15 cm³·mol⁻¹·K) of one independent Tm(III) ion^[22-23]. $\chi_m T$ decreased with decreasing temperature; reaching 0.57 cm³·mol⁻¹·K at 2 K. The above data analysis indicates that the magnetism of all the complexes exhibits weak antiferromagnetic behavior. From the structural diagrams of the four complexes, it can be seen that the ligands in the complexes are relatively large, resulting in a longer distance between rare earth ions, thus there is almost no magnetic interaction between adjacent rare earth ions. At the same time, rare earth ions are difficult to magnetically interact with neighboring ions due to f-electrons. So $\chi_m T$ of the four complexes decreasing with decreasing temperature is not related to the coupling effect. This trend of change is completely caused by the de-heating population of the Stark energy levels of rare earth ions^[24].

3 Conclusions

In summary, four 1D chain structure isomorphic rare earth complexes have been synthesized by the solvothermal method based on the polyacid ligand (H₂cpna) and rare earth metal ions Dy³⁺, Ho³⁺, Er³⁺, and Tm³⁺. The fluorescence and magnetism of complexes **1-4** were studied at room temperature. The fluorescence test results show that the fluorescence intensities of complexes **1-4** were all lower than that of the ligand, and magnetic results indicate that the magnetism of all four complexes exhibits weak antiferromagnetic

behavior.

References:

- [1] Martins V, Xu J, Wang X L, Chen K Z, Hung I A, Gan Z H, Gervais C, Bonhomme C, Jiang S J, Zheng A M, Lucier B E G, Huang Y N. Higher magnetic fields, finer MOF structural information: ^{17}O solid-state NMR at 35.2 T. *J. Am. Chem. Soc.*, **2020**,**142**:14877-14889
- [2] Baranets S, Bobev S. Caught in action. The late rare earths thulium and lutetium substituting aluminum atoms in the structure of $\text{Ca}_{14}\text{AlBi}_{11}$. *J. Am. Chem. Soc.*, **2021**,**143**:65-68
- [3] Lin L, Li L H, Wu C, Huang Z P, Humphrey M G, Zhang C. Incorporating rare-earth cations with moderate electropositivity into iodates for the optimized second-order nonlinear optical performance. *Inorg. Chem. Front.*, **2020**,**7**:2736-2746
- [4] 孙为银. 配位化学. 2版. 北京: 化学工业出版社, **2010**:123-126
SUN W Y. *Coordination chemistry. 2nd ed.* Beijing: Chemical Industry Press, **2010**:123-126
- [5] 黄佳祥, 赵河, 刘淑芹, 张建军. 基于双核 $\{\text{Zn}_2(\text{COO})_4\}$ 次级构筑单元的二维发光配位聚合物的晶体结构和对 Fe^{3+} 的检测. *无机化学学报*, **2021**,**37**(8):1513-1518
HUANG J X, ZHAO H, LIU S Q, ZHANG J J. Two-dimensional luminescent coordination polymer based on dinuclear $\{\text{Zn}_2(\text{COO})_4\}$ second building units: Crystal structure and detection of Fe^{3+} . *Chinese J. Inorg. Chem.*, **2021**,**37**(8):1513-1518
- [6] Thielemann D T, Wagner A T, Rösch E, Kölmel D K, Heck J G, Rudat B, Neumaier M, Feldmann C, Schepers U, Bräse S, Roesky P W. Luminescent cell-penetrating pentadecanuclear lanthanide clusters. *J. Am. Chem. Soc.*, **2013**,**135**:7454-7457
- [7] Liu Y C, Lin P, Du S W. Two novel homochiral enantiomorphanic 3D metal-organic frameworks: Synthesis, crystal structure, luminescent and SHG properties. *Chin. J. Struct. Chem.*, **2013**,**10**:1509-1516
- [8] 李和川, 李明凤, 何成, 段春迎. 基于非贵金属镍的金属有机大环的光解水放氢性能. *无机化学学报*, **2018**,**34**(1):11-19
Li H C, Li M F, He C, DUAN C Y. Construction of a noble-meta-free nickel metal-organic macrocycle for photocatalytic hydrogen production. *Chinese J. Inorg. Chem.*, **2018**,**34**(1):11-19
- [9] Allendorff M D, Bauer C A, Bhakta R K. Luminescent metal-organic frameworks. *Chem. Soc. Rev.*, **2009**,**38**:1330-1352
- [10] Liu S J, Han S D, Zhao J P, Xu J L, Bu X H. In-situ synthesis of molecular magnetorefrigerant materials. *Coord. Chem. Rev.*, **2019**,**394**:39-52
- [11] Gao X S, Ding M J, Zhang J, Zhao L D, Ren X M. Phase selectivity and tunable photophysical nature of rare earth metal-organic frameworks of $\text{Eu}_x\text{Y}_{1-x}$ -PTC ($\text{H}_3\text{PTC}=\text{2,4,6}$ -pyridine tricarboxylic acid; $x=0-1$). *Dalton Trans.*, **2020**,**49**:14985-14994
- [12] Gu J Z, Liang X X, Cai Y, Wu J, Shi Z F, Kirillov A M. Hydrothermal assembly, structures, topologies, luminescence, and magnetism of a novel series of coordination polymers driven by a trifunctional nicotinic acid building block. *Dalton Trans.*, **2017**,**46**:10908-10925
- [13] Shen Z, Zhao Q, Xie H Q, Feng Y Q, Chen S Y, Shi, Z. Synthesis, optical and magnetic research of nicotinic acid ligand Zn, Cd, Mn and Co complexes. *J. Solid State Chem.*, **2021**,**302**:122437-122443
- [14] Sheldrick G M. *SADABS, Area - detector absorption correction*. Siemens Industrial Automation, Inc., Madison, WI, **2001**.
- [15] Sheldrick G M. *SHELXL-2018, Program for X-ray crystal structure solution*. University of Göttingen, Germany, **2018**.
- [16] Chen G J, Gao C Y, Tian J L, Tang J K, Gu W, Liu X. Coordination-perturbed single-molecule magnet behavior of mononuclear dysprosium complexes. *Dalton Trans.*, **2011**,**40**:5579-5583
- [17] Zhang Z Q, Wang P Y, Rong HW, Li L W. Structural and cryogenic magnetic properties of $\text{RE}_2\text{Ni}_2\text{In}$ ($\text{RE}=\text{Pr}$, Nd , Dy and Ho) compounds. *Dalton Trans.*, **2019**,**48**:17792-17799
- [18] Rasamsetty A, Das C, Sañudo E C, Shanmugam M, Baskar V. Effect of coordination geometry on the magnetic properties of a series of Ln_2 and Ln_4 hydroxo clusters. *Dalton Trans.*, **2018**,**47**:1726-1738
- [19] Latendresse T P, Vieru V, Upadhyay A, Bhuvanesh N S, Chibotaru L F, Nippe M. Trends in trigonal prismatic Ln -[1]ferrocenophane complexes and discovery of a Ho^{3+} single-molecule magnet. *Chem. Sci.*, **2020**,**11**:3936-3951
- [20] Gavrikov AV, Koroteev P S, Efimov N N, Dobrokhotova Z V, Ilyukhin A B, Kostopoulos A K, Ariciub A M, Novotortsev V M. Novel mononuclear and 1D-polymeric derivatives of lanthanides and (η^6 -benzoic acid) tricarbonylchromium: Synthesis, structure and magnetism. *Dalton Trans.*, **2017**,**46**:3369-3380
- [21] Wang J, Miao H, Xiao Z X, Zhou Y, Deng L D, Zhang Y Q, Wang X Y. Syntheses, structures and magnetic properties of the lanthanide complexes of the pyrimidyl-substituted nitronyl nitroxide radical. *Dalton Trans.*, **2017**,**46**:10452-10461
- [22] Huizi-Rayo U, Zabala-Lekuona A, Terenzi A, Cruz C. M, Cuerva J M, Rodríguez - Diéguez A, García J A, Seco J M, Sebastian E S, Cepeda J. Influence of thermally induced structural transformations on the magnetic and luminescence properties of tartrate-based chiral lanthanide organic-frameworks. *J. Mater. Chem. C*, **2020**,**8**: 8243-8256
- [23] Anwar M U, Dawe L N, Tandon S S, Bungec S D, Thompson L K. Polynuclear lanthanide (Ln) complexes of a tri-functional hydrazone ligand mononuclear (Dy), dinuclear (Yb , Tm), tetranuclear (Gd), and hexanuclear (Gd , Dy , Tb) examples. *Dalton Trans.*, **2013**,**42**:7781-7794
- [24] Kahn O. *Molecular magnetism*. Weinheim, New York: VCH-Verlag, **1993**:43-51